Three-Dimensional Adaptive Grid Method

Kazuhiro Nakahashi* and George S. Deiwert†
NASA Ames Research Center, Moffett Field, California

A three-dimensional solution adaptive grid scheme suitable for complex fluid flows is described. This method, using tension and torsion spring analogies, was previously developed and successfully applied for two-dimensional flows. In the present work, a collection of three-dimensional flowfields is used to demonstrate the feasibility and versatility of this concept to include an added dimension. Flowfields considered include: 1) supersonic flow past an aerodynamic afterbody with a propulsive jet at incidence to the freestream, 2) supersonic flow past a blunt fin mounted on a solid wall, and 3) supersonic flow over a bump. In addition to generating three-dimensional solution-adapted grids, the method can also be used effectively as an initial grid generator. The utility of the method lies in: 1) optimum distribution of discrete grid points, 2) improvement of accuracy, 3) improved computational efficiency, 4) minimization of data-base sizes, and 5) simplified three-dimensional grid generation.

Introduction

An important subject to study in computational fluid dynamics is solution adaptive grid methods, due to their potential for improving the efficiency and accuracy of numerical methods. The use of adaptive grids can be expected to help minimize computer memory and speed requirements, particularly for three-dimensional flowfield computations.

Many solution adaptive grid methods have been proposed and are well reviewed by both Anderson[1] and Thompson.[2] One of the most popular of these methods is based on an equidistribution concept,[3-5] i.e., redistribution of grid points such that a positive weighting function, w_i, is equally distributed over a coordinate line:

$$w_i \Delta s_i = C \tag{1}$$

where Δs_i is the grid interval and C is a constant. This is essentially a one-dimensional approach. For two-dimensional problems, this scheme is applied with the grid points constrained to move along one family of fixed coordinate lines.

Although schemes using one-directional adaptation along a fixed family of coordinate lines have been successfully applied to two-dimensional flow problems, a major deficiency is a lack of the control of grid skewness. When grids become highly skewed, truncation error is increased. To avoid excessive skewness, grid-point distribution must somehow be affected by near neighbors in each direction. This is the key point in determining whether the one-dimensional equidistribution scheme can be extended satisfactorily to multidimensional problems.

Several improvements of the equidistribution scheme have been proposed.[6,7] In these schemes an orthogonality constraint is used to control the grid distribution in a two-dimensional field whereby the grids are adapted in one dimension and orthogonality is imposed on the second.

A more practical adaptive grid scheme was developed by the present authors.[8] This scheme is based on a tension and torsion spring analogy such that each grid point is imagined to be suspended by tension springs and torsion springs. The grid is optimally redistributed by minimizing the energy of this system of springs. Tension springs, which connect adjacent grid points along coordinate lines, control grid spacings. This concept corresponds to the equidistribution scheme. The torsion springs, which are attached to each grid node, control inclinations of coordinate lines and prevent excessive grid skewness. This torsion spring concept couples the information of near neighbors so that the distribution of points in the multidimensional field can retain a degree of smoothness. To reduce complexity and eliminate the elliptic behavior of the resulting system of equations, the coupling of information is constrained to be one-sided. Thus the grid distribution is determined in a parabolic manner, which simplifies the solution procedures and reduces the computational time. Two-directional grid adaptation is efficiently achieved by splitting the solution procedure into a sequence of unidirectional adaptations.

These features make this adaptive grid method practical and robust, and the scheme has been successfully applied to the problems of two-dimensional, transonic and supersonic airfoil flowfields and axisymmetric, supersonic afterbody flowfields with propulsive jets.[9] These results show that shock waves and free shear layers are clearly described by clustering the grid points near those regions. The significant improvements of the accuracy of the solutions and the efficiency of computation confirm the usefulness of the adaptive grid scheme.

The principal purpose of this paper is to extend the method to three dimensions. The control of grid skewness by two torsion springs, as well as control of spacings by the tension springs, will appropriately distribute grid points on each coordinate line in the three-dimensional flowfield. A collection of three-dimensional flows is used to demonstrate the feasibility and versatility of this method to a variety of complex flows, including: 1) supersonic flow past an aerodynamic afterbody with a propulsive jet at incidence of the freestream,[10] 2) supersonic flow past a blunt fin mounted on a solid wall,[11] and 3) supersonic flow over a bump.[12] All of these cases are supersonic viscous flows and there are shock waves and shear layers whose locations are not known a priori, necessitating the adaptive grid method.

A secondary, although important, purpose of this paper is to describe the use of this adaptive grid method as an effective initial grid-generation scheme. The mesh spacings are easily controlled in a three-dimensional field by replacing the flow property driving the adaptation with specific geometry functions.

The utility of the method lies in 1) optimum distribution of discrete grid points in a three-dimensional field, 2) im-

Presented as Paper 85-0486 at the AIAA 23rd Aerospace Sciences Meeting, Reno, NV, Jan. 14-17, 1985; received Jan. 30, 1985; revision received Oct. 1, 1985.

*NRC Research Associate. Member AIAA.
†Research Scientist. Member AIAA.

provement of accuracy, 3) improved computational efficiency, 4) minimization of data-base sizes, and 5) simplified three-dimensional grid generation.

One-Directional Adaptation

Basic Equations of Grid Adaptation

For simplicity of illustration, consider a three-dimensional flowfield with adaptation in one direction. In Fig. 1, grid points on the $\zeta_{i,j}$ coordinate are free to move along a line whose configuration is fixed. Grid point A on the $\zeta_{i,j}$ coordinate is suspended by two tension springs which connect point A to points B and C, and whose spring constants are $w_{i,j,k-1}$ and $w_{i,j,k}$. To distribute grid points along the $\zeta_{i,j}$ coordinate line in proportion to the flow property gradients, the relationship between the tension spring constant w and the gradient of the dependent variable f is given by

$$w_{i,j,k} = F_{i,j,k} + C_1 \left| f_{i,j,k+1} - f_{i,j,k} \right| / (s_{i,j,k+1} - s_{i,j,k}) \tag{2}$$

where C_1 is a constant coefficient, and $s_{i,j,k}$ the arc length calculated from point $(i,j,1)$ along the $\zeta_{i,j}$ coordinate. In actual practice, $s_{i,j,k}$ is approximated by arc secants for simplicity. $F_{i,j,k}$ is used to maintain grid smoothness and has a value of 1 in most cases. When the coefficient C_1 is set to zero, this will result in grids with a uniform distribution of arc length along a grid line. However, if grid spacings at both ends of the $\zeta_{i,j}$ coordinate are specified and those spacings are much different from each other, $F_{i,j,k}$ can be specified by

$$F_{i,j,k} = a b_{i,j}^{k} \tag{3}$$

where a is a constant and

$$b_{i,j} = (\Delta s_{i,j,M-1} / \Delta s_{i,j,1})^{1/(M-2)} \tag{4}$$

M is the total number of grid points along the coordinate, and $\Delta s_{i,j,1}$ and $\Delta s_{i,j,M-1}$ are grid spacings at both ends. The index, k, is used as an exponent for $b_{i,j}$ and, if the flow gradients are zero along the coordinate line, or if the coefficient C_1 is zero, the term F given in Eq. (3) produces an exponentially stretched grid distribution. This can be useful for generating grids for viscous flow computations and can be used to cluster points near wall boundaries. This formulation for F will be discussed in more detail later. When Eq. (3) is used in conjunction with the dependent variable gradient in Eq. (2), the grid can be clustered near boundaries as well as near high gradient regions within the flowfield.

A force of control inclinations of the ξ and η coordinates is given by the two torsion springs attached at points D and E in Fig. 1. These torsion springs enforce the inclinations of lines $\overline{DA}$ and $\overline{EA}$ with respect to prescribed reference lines. If the coefficients for the torsion springs are denoted by C_{21} and C_{22}, a mathematical statement of the force is given by

$$F_{\text{torsion}} = -C_{21}(\theta_{i-1,j,k} - \phi_{i-1,j,k}) - C_{22}(\theta_{i,j-1,k} - \phi_{i,j-1,k}) \tag{5}$$

where $\theta_{i-1,j,k}$ and $\theta_{i,j-1,k}$ are inclinations of lines $\overline{DA}$ and $\overline{EA}$, and $\phi_{i-1,j,k}$ and $\phi_{i,j-1,k}$ the inclinations of the reference lines. The reference line for line $\overline{DA}$ can be prescribed in a variety of ways. For example, 1) as an extension of $\overline{FD}$ in the ξ-ζ plane to maintain smoothness in the ξ line, 2) a line normal to the $\zeta_{i,j}$ coordinate in the ξ-ζ plane to make the grid quasiorthogonal, or 3) a streamline in the ξ-ζ plane so that the grid follows the flow, etc. In practical calculations, a combination of these reference lines is used. The reference line for $\overline{EA}$ can be prescribed similarly.

The distribution of grid points along the $\zeta_{i,j}$ coordinate, i.e., new values of $s_{i,j,k}$, is determined by a balance equation for the complete spring system:

$$\begin{aligned} &w_{i,j,k}(s_{i,j,k+1} - s_{i,j,k}) - w_{i,j,k-1}(s_{i,j,k} - s_{i,j,k-1}) \\ &\quad - C_{21}(\theta_{i-1,j,k} - \phi_{i-1,j,k}) - C_{22}(\theta_{i,j-1,k} - \phi_{i,j-1,k}) = 0 \end{aligned} \tag{6}$$

To facilitate solutions of Eq. (6), the third and fourth terms are rewritten as

$$\begin{aligned} C_{21}(\theta_{i-1,j,k} - \phi_{i-1,j,k}) &\Rightarrow T_{i-1,j,k}(s_{i,j,k} - \bar{s}_{i,j,k}) \\ C_{22}(\theta_{i,j-1,k} - \phi_{i,j-1,k}) &\Rightarrow T_{i,j-1,k}(s_{i,j,k} - \tilde{s}_{i,j,k}) \end{aligned} \tag{7}$$

where $\bar{s}_{i,j,k}$ and $\tilde{s}_{i,j,k}$ are arc lengths to the intersections of reference lines $\overline{DA'}$ and $\overline{EA''}$, respectively, with the $\zeta_{i,j}$ coordinate as depicted in Fig. 2. The $T_{i-1,j,k}$ and $T_{i,j-1,k}$ terms are set equal to C_{21} and C_{22} divided by lengths of $\overline{DA'}$

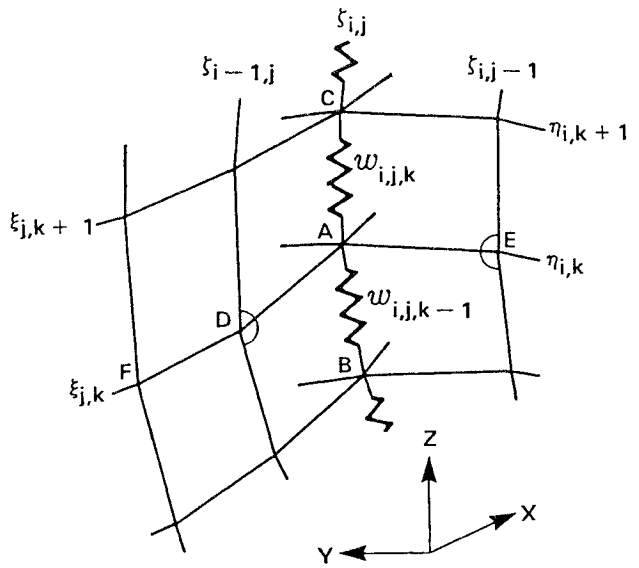

Fig. 1 Adaptive grid algorithm with tension and torsion spring analogy.

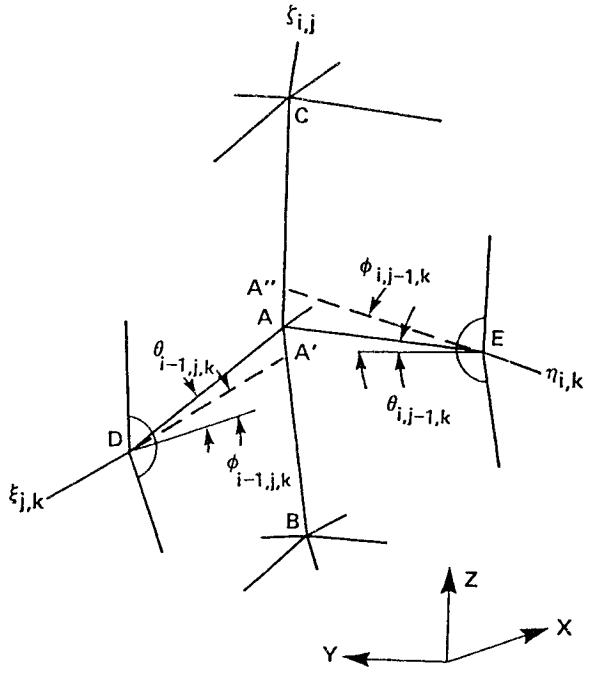

Fig. 2 Notation for torsion spring analogy.

and $\overline{EA''}$. Finally, Eq. (6) reduces to

$$w_{i,j,k-1}s_{i,j,k-1} - (w_{i,j,k} + w_{i,j,k-1} + T_{i-1,j,k} + T_{i,j-1,k})s_{i,j,k} + w_{i,j,k}s_{i,j,k+1} = -T_{i-1,j,k}\bar{s}_{i,j,k} - T_{i,j-1,k}\tilde{s}_{i,j,k} \quad (8)$$

This is a tridiagonal system of equations for $s_{i,j,k}$ and can be solved readily.

In this analysis only the torsion forces on the upstream sides ($\zeta_{i-1,j}$) and ($\zeta_{i,j-1}$) influence the distribution at the $\zeta_{i,j}$ coordinate. This permits simple marching schemes to be used without any loss of generality, and contributes to the simplicity and robustness of the method. Conversely, if the influence from both sides ($\zeta_{i-1,j}$, $\zeta_{i+1,j}$, $\zeta_{i,j-1}$, and $\zeta_{i,j+1}$) is considered simultaneously, Eq. (8) is no longer a tridiagonal system of equations and the computational effort is increased considerably without any additional benefit. In addition, note that the downstream influence ($\zeta_{i+1,j}$ and $\zeta_{i,j+1}$) could be used instead of the upstream, without any additional complexity or loss of generality.

One-Directional Adaptation Procedure

The procedure for grid adaptation of a three-dimensional flowfield solution along ζ coordinate lines is as follows:

1) Specify the region in computational space to be adapted, i_S, i_E, j_S, j_E, k_S, and k_E, where the subscripts S and E denote starting and ending indices of the selected region.
2) Specify the tension spring coefficient C_1, and the torsion spring coefficients C_{21} and C_{22}.
3) March in the j direction beginning at j_S.
4) For each j, march in the i direction beginning at i_S.
5) For each i and j, calculate arc lengths $s_{i,j,k}$.
6) Calculate $w_{i,j,k}$ from Eq. (2).
7) Calculate $\bar{s}_{i,j,k}$, $\tilde{s}_{i,j,k}$, $T_{i-1,j,k}$, and $T_{i,j-1,k}$.
8) Correct any overlapping of $\bar{s}_{i,j,k}$ and $\tilde{s}_{i,j,k}$.
9) Solve the tridiagonal system of equations, Eq. (8), for new values of $s_{i,j,k}$.
10) Interpolate $f_{i,j,k}$ on $s_{i,j,k}$ from the flow solution data on the old grid points.
11) Check the convergence of $s_{i,j,k}$. If not converged, return to step 6.

In step 1, the region for grid adaption is specified; it is not always necessary to adapt the grid for the entire flowfield, and it may be more efficient to select subdomains as suggested in Fig. 3. When adapting in subdomains, two concerns must be addressed. One is that when a marching procedure is used, the region downstream of the subdomain, $i_S \le i \le i_E$, $j_E < j \le j_{\max}$, $k_S \le k \le k_E$, and $i_E < i \le i_{\max}$, $j_S \le j \le j_{\max}$, $k_S \le k \le k_E$, must also be modified. This can be affected by using the spacing ratio on the last line of the subdomain as a condition for downstream redistributions. The other concern is to avoid large differences in spacing at the subdomain boundaries, i.e., between $\Delta s_{i,j,k_S}$ and $\Delta s_{i,j,k_S-1}$, and between $\Delta s_{i,j,k_E-1}$ and $\Delta s_{i,j,k_E}$. These differences arise when the mesh spacing inside the subdomain is determined by the spring balance equation, Eq. (8), while outside the mesh spacing remains fixed. This spacing difference can be alleviated by modifying the tension spring constants near the subdomain boundary. If we consider a tension spring system only, the ratio of the spacing is equal to the inverse ratio of the tension spring constant, i.e., $\Delta s_{i,j,k}/\Delta s_{i,j,k+1} = w_{i,j,k+1}/w_{i,j,k}$. Thus, $\Delta s_{i,j,k_S}$ can be modified iteratively by

$$w_{i,j,k_S}^{(N+1)} = w_{i,j,k_S}^{(N)}[\Delta s_{i,j,k_S}^{(N)}/\Delta s_{i,j,k_S-1}^{(N)}] \quad (9)$$

$w_{i,j,k}$ near w_{i,j,k_S} is also modified:

$$w_{i,j,k_S+m}^{(N+1)} = (m/4)w_{i,j,k_S+m}^{(N)} + (1-m/4)w_{i,j,k_S}^{(N)} \quad (10)$$

for $1 \le m \le 3$.

If the grid adaptation is started from a boundary, i.e., $i_S = 1$ or $j_S = 1$, the grid-point distribution along the ζ coordinate is determined by solving Eq. (8) without a torsion spring on that boundary; namely with C_{21} or C_{22} set equal to zero, respectively, at that boundary.

It may be desirable to filter or smooth the distribution of tension spring constants $w_{i,j,k}$ to achieve a smooth variation along coordinate lines. This smoothing can be done using

$$w_{i,j,k} = (w_{i,j,k-1} + w_{i,j,k} + w_{i,j,k+1})/3 \quad (11)$$

For "noisy" flow solutions, the flow property $f_{i,j,k}$ in Eq. (2) may also be smoothed along a line.

If we consider tension springs only, $s_{i,j,k}$ determined by Eq. (8) is always a monotonically increasing function along a line. However, with the introduction of a torsion force it is possible for the grid points to cross or overlap. To avoid such overlapping, $\bar{s}_{i,j,k}$ and $\tilde{s}_{i,j,k}$ must be monitored to determine if they are monotonically increasing. If they do not, the values of $\bar{s}_{i,j,k}$ and $\tilde{s}_{i,j,k}$ can be modified to be equal to the average value of the local maximum and minimum values of $\bar{s}_{i,j,k}$ and $\tilde{s}_{i,j,k}$ in the overlapping region in order to ensure that $\bar{s}_{i,j,k} \le \bar{s}_{i,j,k+1}$ and $\tilde{s}_{i,j,k} \le \tilde{s}_{i,j,k+1}$.

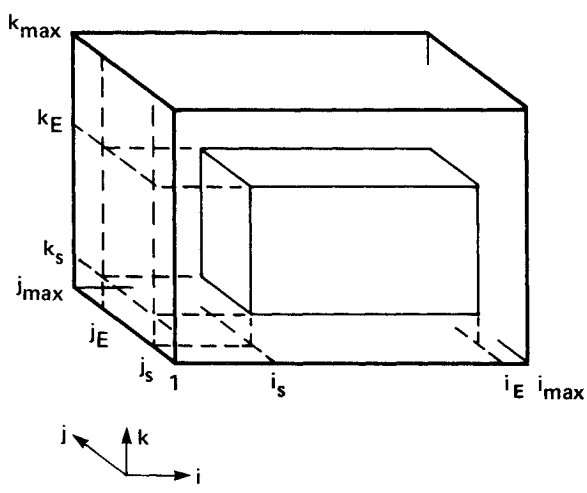

Fig. 3 Adaptive grid subdomain in the entire field.

Three-Directional Adaptations

A model using tension and torsion springs for a three-dimensional adaptation can be depicted as a spring system in which each grid node is suspended by six tension and twelve torsion springs. To adapt the grid in all three directions simultaneously is a complex task, and requires significant computational effort. To minimize this complexity, the procedure is split into a sequence of one-directional adaptations in which three-dimensional grid movement is achieved by successive applications of the one-directional method. For example, grid points are first adapted to the solution along each ζ coordinate whose configuration is fixed, followed by adaptation along each η coordinate, and then for each ξ coordinate. This is analogous to the factored ADI schemes for partial differential equations. It is not particularly necessary to achieve convergence in this adaptation procedure and, in fact, one iteration is generally sufficient in practical applications of the scheme. While the selected ordering of the coordinate adaptation is arbitrary, the resulting adapted grid will be unique for each possible split sequence. In general, choosing the first adaptation along the coordinate for which gradients of flow properties are large will produce good results.

The solution field is interpolated into the newly adapted grid, using second-order, one-dimensional Lagrange interpolation after each one-directional adaptation. This interpolation is performed after each one-directional adaptation and is a more efficient process than using multidimensional

interpolations. The successive application of one-directional adaptation also enhances the versatility of the method in that unidirectional adaptation can be used in regions where gradients are large in one direction only. If time accuracy is necessary for unsteady flow, grid speeds can be evaluated after adaptation.

Selection of Parameters

Control Constants

There are four coefficients that control the grid distribution. The tension spring coefficient C_1 affects the mesh spacing along each line. This coefficient should be selected to provide adequate clustering in high gradient regions without voiding the low gradient regions. A guideline for selecting the tension spring coefficient can be given by considering the ratio of the maximum spacing, $\max[\Delta s]$, to the minimum spacing, $\min[\Delta s]$, along a line. Neglecting torsion springs and the smoothness term F, this ratio corresponds to the ratio of minimum and maximum tension spring constants, $\min[K]/\max[K]$, and the minimum mesh spacing is somewhat controlled by choosing C_1 as

$$C_1 = (A-1)\Big/\left(\max\frac{\partial f}{\partial s} - \min\frac{\partial f}{\partial s}\,A\right) \tag{12}$$

where

$$A = (\min[\Delta s]/\max[\Delta s])_{\text{specified}}$$

The relation between the tension and torsion forces is determined by coefficients C_{21} and C_{22}. If values for these coefficients are large, the tension spring system is highly damped and the ξ and η coordinate lines are enforced to their reference values. If these values are small, the tension spring system is relatively undamped and the coordinate lines may oscillate. This will increase the number of iterations required to achieve a desired convergence. The values used in the examples described in the following section are between $C_1/2$ to $C_1/20$; i.e., $C_1/2 \geq (C_{21}, C_{22}) \geq C_1/20$.

To enforce near-orthogonality, or to avoid a rapid change in curvature, the large values of C_{21} and C_{22} should be used. The orthogonality condition may be desirable near flowfield boundaries, and a gradual change in curvature may be desirable near subdomain starting boundaries.

The constant a in Eq. (3) should be chosen such that the maximum value of $F_{i,j,k}$ is the same order as the maximum of the flow variable gradient term; the second term on the right-hand side of Eq. (2). A simple method to assure this character is to simply define a by an equality between the maxima of these two terms.

Selection of Flow Properties

The selection of the flow properties to drive the grid adaptation is considered next. Ideally, it is desirable to minimize the truncation error and distribute the error uniformly over the computational domain. In a practical sense, however, the truncation error cannot be estimated accurately and, in general, will be noisy. Typically, the error is greatest in regions where the flowfield gradients are large. This is true until an overclustering of grid points is achieved, which generally never occurs for flowfields with discontinuities such as shocks and slip surfaces. Hence, a more practical property to drive the adaptation is one that can identify such high gradient regions as shocks, slip surfaces, and free shear layers. While any flowfield property, or combination of properties, can be used, some are more general and are better descriptors than others. For the compressible flowfields considered in this study, the density gradient was found to be a suitable driver. It is capable of identifying both shocks and slip surfaces, but not attached shear layers. Pressure gradients, on the other hand, will identify shocks but will not identify slip surfaces at all. The user must exercise some discretion in the selection of the adaptive grid driving function to realize his desired objectives.

Results

Afterbody Flowfield

First, as an example, is a supersonic flow past an aerodynamic afterbody, with a propulsive jet, at an incidence of 6 deg to the freestream of Mach 2. The jet-exit Mach number is 2.5 at a static pressure three times that of the freestream. This is a complex flow and contains regions of strong viscous-inviscid and strong viscous-viscous interactions. The supersonic external flow contains compression shocks, as well as regions of rapid expansion. The boundary layer on the afterbody leaves as a free shear and merges with the shear layer between the propulsive jet and the external flow. The underexpanded propulsive jet exhibits internal structures in the form of barrel shocks and Mach disks. These discontinuous flow regions require a high degree of resolution to be captured clearly. The locations of these high gradient regions are not generally known a priori and it is necessary to adapt the grid to the solution to assure the accurate capturing and resolution of these features. (This flowfield was the original motivation for the development of this solution adaptive grid study.)

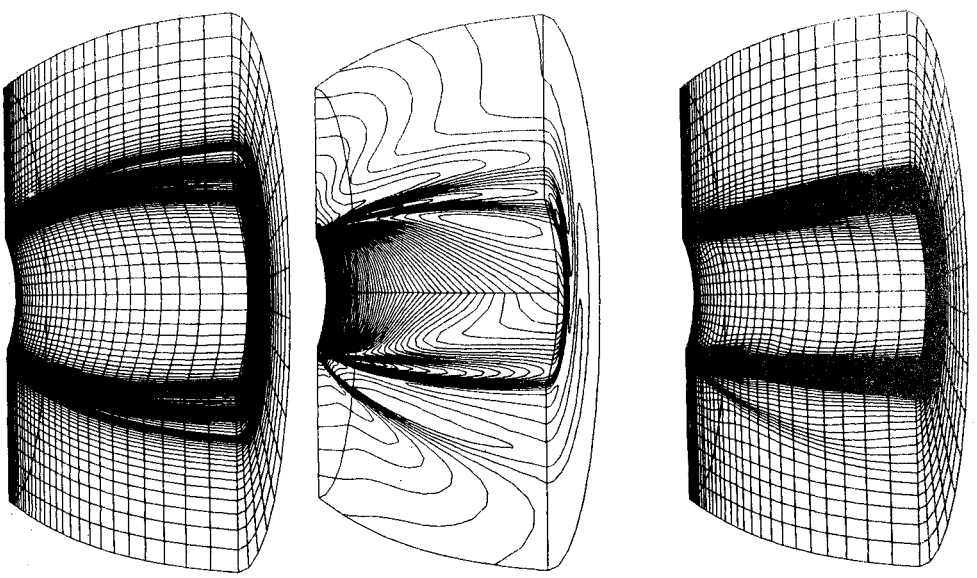

a) Initial grid. b) Computed isopycnics with initial grid. c) Adapted grid.

Fig. 4 Grids and isopycnics in a jet-exit segment of the afterbody flowfield.

Shown in Fig. 4 is a lateral perspective of the jet-exit plume and the near external flow region just downstream of the afterbody. This is a $30\times80\times20$ segment of the complete $140\times100\times20$ computational domain. Shown is the bilateral plane of symmetry (30×80) and the downstream axial plane (80×20) of the segment. The initial grid ($140\times100\times20$) was generated by an algebraic method, a segment of this grid is shown in Fig. 4a. These grid points were clustered along free shear layers whose positions were determined from schlieren photographs of an experiment run at a jet-to-freestream static-pressure ratio of 9; the computations were performed for a ratio of 3. Hence, the grid-point location is not truly appropriate for the computed flow conditions. Shown in Fig. 4b are density contours computed by Deiwert and Rothmund[10] using the thin-layer, approximated, time-dependent, compressible, Reynolds-averaged Navier-Stokes equations.

The initial grid was readapted to the density gradient of the three-dimensional solution in the radial (j-index) and circumferential (k-index) directions. Although the grid can be adapted for each of the three directions, adaptation in the streamwise (i-index) direction, where the gradients are small, was not considered relevant in this problem. Shown in Fig. 4c is the adapted grid of the same ($30\times80\times20$) segment. In the radial direction the adapting procedure was started at the third ξ-constant plane from the end of body and marched downstream. In each ξ-constant plane, circumferential marching from the leeward to windward was used.

These results show that the adapted grid points are clustered to the regions of free shear layers, barrel shocks, oblique shocks, and rapid expansions. In the circumferential direction, grid points have been adjusted somewhat windward to better resolve the compressive shock front. This front does not extend totally leeward. Figure 5 shows enlarged views of density contours and corresponding adapted grids in the windward near base region. Even though the computed discontinuities are sharply delineated, as shown in Fig. 5a, and there is rapid and dramatic variation in flowfield properties in the near base region, the adapted grid retains a sufficient degree of smoothness; a result of the torsion spring concept.

It has been shown for axisymmetric studies[9] that the significant improvement in the quality of computational results can be expected by using grid adaptation. There is every reason to expect similar improvement for full three-dimensional studies.

Blunt Fin Mounted on a Flat Plate

The second example of the three-dimensional adaptive grid application considers the supersonic flowfield around a blunt fin mounted on a flat plate. This flowfield was numerically simulated by Hung and Buning[11] using the thin-layer, time-dependent, compressible, Reynolds-averaged Navier-Stokes equations. A flow with a freestream Mach number of 2.95 and an oncoming boundary-layer thickness δ/D of 0.1 are considered to demonstrate the adaptive grid.

The initial grid was adapted to the solution in both the k- and j-index directions. Density was used as the parameter to drive the adaptation, except in the region upstream of the normal shock wave near the flat plate where pressure was used. The flow solver used is a finite-volume method, and the computed flow properties for the centroid of each volume element were three dimensionally interpolated onto the volume element vertices before adaptation. After the adaptation, the flow properties at each adapted node were restored to the centroid of each volume element for the next flowfield computations.

Shown in Fig. 6a is the resulting adapted grid which clearly indicates a clustering to regions containing a normal shock, an oblique shock, and a separated shear layer. The flowfield was recomputed using this adapted grid. Figure 6b shows computed density contours using the adapted grid.

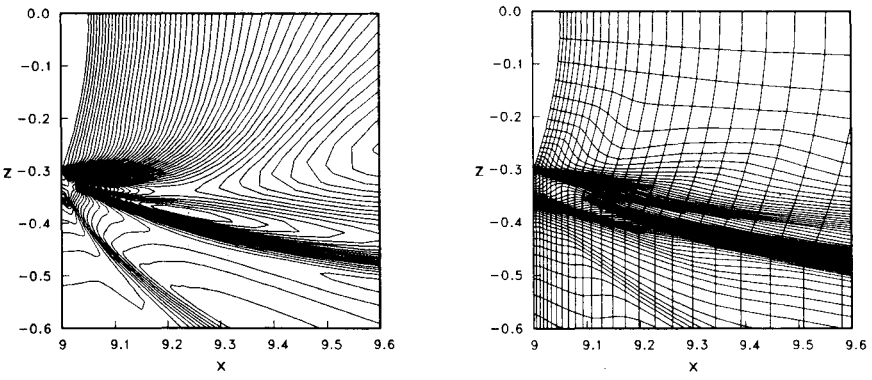

a) Computed isopycnics with initial grid.

b) Adapted grid.

Fig. 5 Jet-exit region detail of isopycnics and adapted grid.

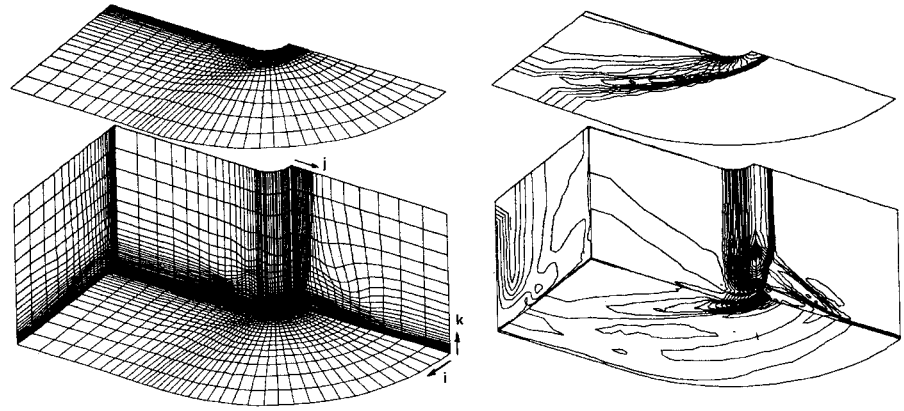

a) Adapted grid.

b) Computed isopycnics with adapted grid.

Fig. 6 Grid and isopycnics for blunt fin flowfield.

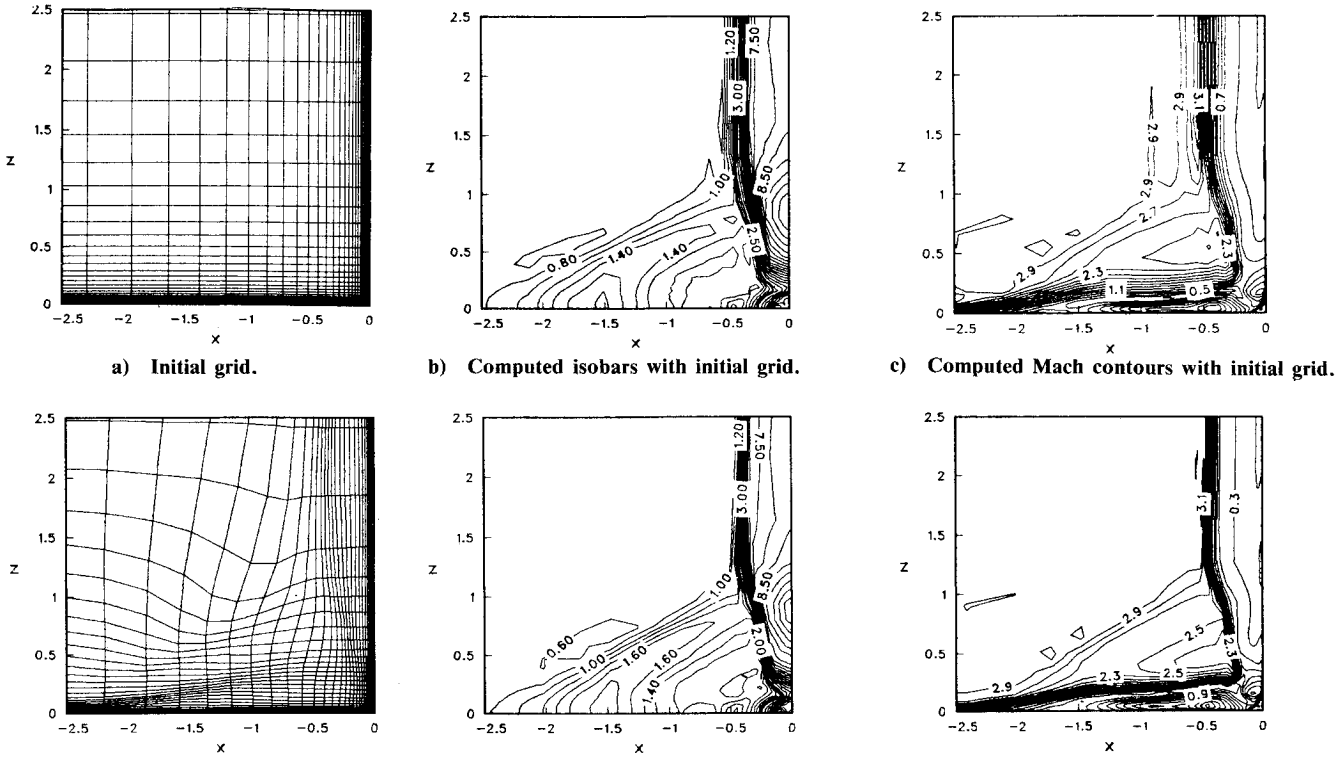

Fig. 7 Grids, isobars, and Mach contours on plane of symmetry in front of the blunt fin.

Sharper shocks and shear layers can be observed in front of the blunt fin.

Shown in Fig. 7 are detailed plots on the plane of symmetry of the blunt fin. Shown in Fig. 7a is the initial grid, and in Fig. 7d the adapted grid. Pressure contours (Figs. 7b and 7c) indicate a crisper normal shock in front of the fin on the adapted grid (Fig. 7e), and also a crisper oblique shock wave caused by the separated shear layer. The peak pressure on the blunt fin, due to the incident separation shock, is higher using the adapted grid. Crisper shock waves are also shown in the Mach contours in Figs. 7c and 7f. Here, the separated shear layer is better resolved in the figure for the adapted grid.

Initial Grid Generation—Flow Past a Bump

The application of the scheme to three-dimensional grid generation is described here. If the function f in Eq. (2) is specified explicitly, as a function of geometry, the adaptive grid method can be used as a grid-generation code. Shown in Fig. 8 is a pictorial sequence of an example describing the procedure for a three-dimensional flowfield computation beginning with the initial grid generation. The flow past a bump was used for this example and has been computed and discussed in detail by Horikawa,[12] who solved the thin-layer, time-dependent, compressible, Reynolds-averaged Navier-Stokes equations.

Initially, a rectangular grid ($49\times29\times40$) is generated with uniform spacings on each side of a rectangular parallelepiped. One surface of the rectangular parallelepiped is then deformed to describe a bump by shortening the z coordinate in a prescribed manner, Fig. 8a. The shape of the bump is defined by

$$z(x,y)=0.25[\sin(4\pi(x-0.5)-0.5\pi)+1][\cos(4\pi y)+1],$$
$$\text{for } 0.5\le x\le 1 \text{ and } 0\le y\le 0.25$$
$$=0, \quad \text{for } x\le 0.5 \text{ or } 1\le x \text{ 0r } 0.25\le y \tag{13}$$

This grid is then redistributed successively in each coordinate direction. Considering the i direction first, the function f is given by

$$f_{i,j,k}=z_{i-1,j,k}-2z_{i,j,k}+z_{i+1,j,k} \tag{14}$$

This expression for f clusters the grid points to regions of large curvature of the ξ coordinate in the x-z plane. The mesh spacings of both ends, $\Delta x_{1,j,k}=x_{2,j,k}-x_{1,j,k}$ and $\Delta x_{i_{\max}-1,j,k}=x_{i_{\max},j,k}-x_{i_{\max}-1,j,k}$, is also specified. In the j direction, f is specified by the similar expression to Eq. (14) in the y-z plane. Again, end spacings are specified and Eqs. (2-4) are used to exponentially distribute the points in the plane of symmetry. In the k direction, f is set equal to zero and Eqs. (2-4) are used to cluster points near the wall surface.

The grid-line inclinations are controlled by using larger relative values for torsion springs to make the grid quasi-orthogonal. This orthogonality is enchanced near the bump on the wall by increasing the torsion spring coefficients. As shown in Fig. 8b, the grid spacings and grid-line inclinations are generically clustered in all three directions. In general, it is easier to control the grid using the scheme rather than using elliptic methods; the generality available is greater than with algebraic methods.

The resulting initial grid is subsequently adapted to the solution during the course of reaching a steady state, by replacing the specified function f, used initially to generate the grid, with density.

Figure 8c shows computed density contours before grid adaptation. Grid points are then adapted twice in both the j and k directions (Fig. 8d) before obtaining the final solution (see Fig. 8e). This final solution shows a crisper three-dimensional shock surface in front of the bump and a separated shear layer behind the bump.

This consistent procedure of grid generation and flowfield computation considerably reduces the computational effort for the three-dimensional grid generation and flowfield computation and provides accurate solutions with a minimal number of points.

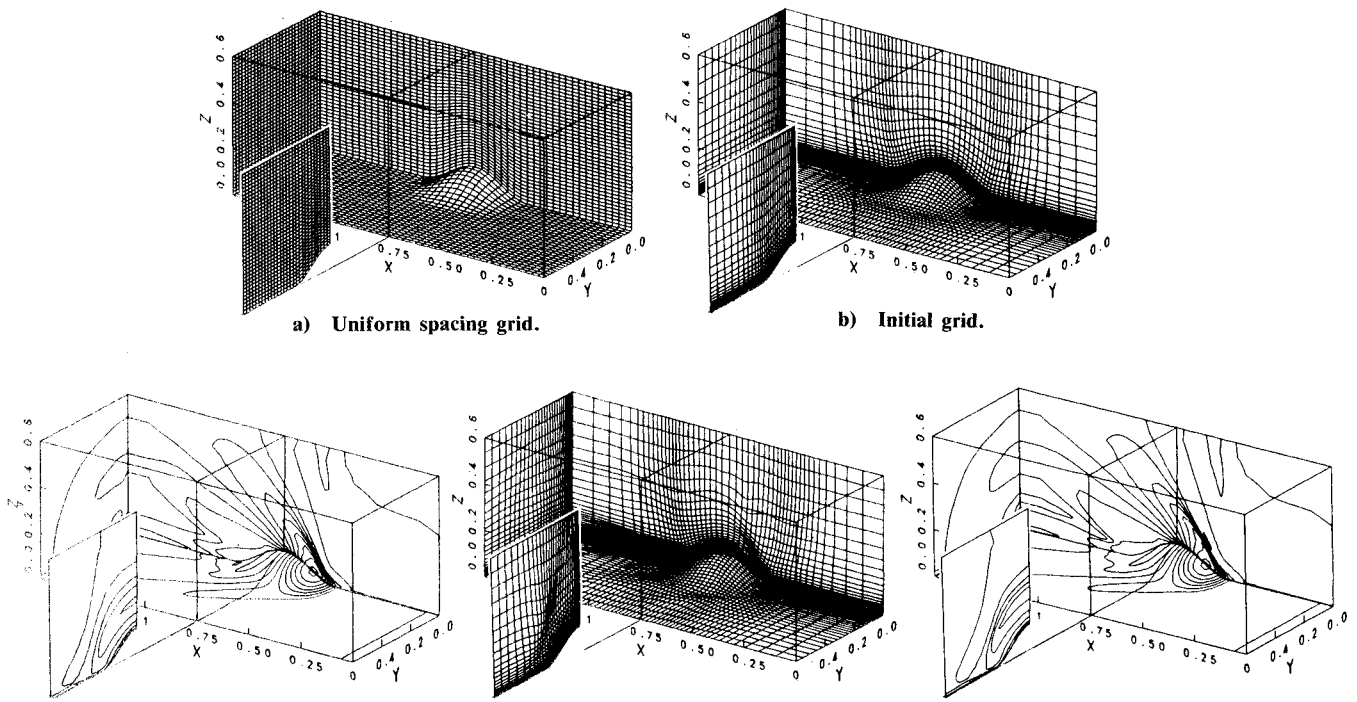

a) Uniform spacing grid. b) Initial grid.

c) Computed isopycnics with initial grid. d) Adapted grid. e) Computed isopycnics with adapted grid.

Fig. 8 Sequence of three-dimensional bump flowfield computation from its initial grid generation.

Summary

The principal feature of the proposed adaptive grid method are:

1) A simple concept consisting of a tension and torsion spring analogy. The combination of these springs produces a suitable adaptive grid without excessive grid skewness in the three-dimensional field.

2) A marching-type calculation procedure that reduces computation time.

3) A simple and practical split-solution procedure for multidirectional adaptation.

4) A method that can be applied independently to subdomains of the complete grid.

5) Control of grid inclination using torsion springs makes it possible to control skewness and generate a nearly orthogonal adaptive grid.

6) Initial grid generation is possible by clustering grid points to specified boundaries and to regions of boundary curvature.

These features make the adaptive grid method practical and robust, and enhance its applicability. This method can be applied to two- and three-dimensional fluid-flow problems without difficulty and requires little computational time and effort.

The computed results using adapted grids show significant improvement in the quality of definition of flow discontinuities such as shock waves and free shear layers.

Acknowledgments

The authors are indebted to C. M. Hung and M. Horikawa for their cooperation in this study. The figures in this paper were generated using a three-dimensional graphics package of P. Buning.

References

[1]Anderson, D. A., "Adaptive Grid Methods for Partial Differential Equations," *Advances in Grid Generation*, edited by K. Ghia and I. Ghia, *Proceedings of the ASME Fluids Engineering Conference*, Houston, TX, 1983, pp. 1-15.

[2]Thompson, J. F., "A Survey of Dynamically-Adaptive Grids in the Numerical Solution of Partial Differential Equations," AIAA Paper 84-1606, 1984.

[3]Rai, M. M. and Anderson, D. A., "Application of Adaptive Grids to Fluid-Flow Problems with Asymptotic Solutions," *AIAA Journal*, Vol. 20, April 1982, pp. 496-502.

[4]Dwyer, H. A., "Grid Adaption for Problems in Fluid Dynamics," *AIAA Journal*, Vol. 22, Dec. 1984, pp. 1705-1712.

[5]Gnoffo, P. A., "A Finite-Volume Adaptive Grid Algorithm Applied to Planetary Entry Flowfields," *AIAA Journal*, Vol. 21, Sept. 1983, pp. 1249-1254.

[6]Anderson, D. A. and Rajendran, N., "Two Approaches Toward Generating Orthogonal Adaptive Grids," AIAA Paper 84-1610, 1984.

[7]Dwyer, H. A. and Onyejekwe, O. O., "Generation of Fully Adaptive and/or Orthogonal Grids," *Proceedings of the Ninth International Conference on Numerical Methods in Fluid Dynamics*, Saclay, edited by Soubbaramayer and Broujot, Springer-Verlag, 1985, pp. 203-207.

[8]Nakahashi, K. and Deiwert, G. S., "A Practical Adaptive Grid Method for Complex Fluid Flow Problems," *Proceedings of the Ninth International Conference on Numerical Methods in Fluid Dynamics*, Saclay, edited by Soubbaramayer and Broujot, Springer-Verlag, 1985, pp. 422-426 also NASA TM-85989, June 1984.

[9]Deiwert, G. S., Andrews, A. E., and Nakahashi, K., "Theoretical Analysis of Aircraft Afterbody Flow," AIAA Paper 84-1524, 1984.

[10]Deiwert, G. S. and Rothmund, H., "Three Dimensional Flow Over a Conical Afterbody Containing a Centered Propulsive Jet: A Numerical Simulation," AIAA Paper 83-1709, 1983.

[11]Hung, C. M. and Buning, P. G., "Simulation of Blunt-Fin Induced Shock Wave and Turbulent Boundary Layer Interaction," AIAA Paper 84-0457, 1984.

[12]Horikawa, M., "Numerical Simulation of the Flow Around a Bump on a Wall," Engineering Thesis, Stanford University, Stanford, CA, Oct. 1984.